Hydrogeol J (2018) 26:133–146
DOI 10.1007/s10040-017-1640-y

PAPER

Improved water resource management for a highly complex environment using three-dimensional groundwater modelling

Christian Moeck[1] · **Annette Affolter**[2] · **Dirk Radny**[1] · **Horst Dressmann**[2] · **Adrian Auckenthaler**[3] · **Peter Huggenberger**[2] · **Mario Schirmer**[1,4]

Received: 19 January 2017 / Accepted: 3 July 2017 / Published online: 2 August 2017
© Springer-Verlag GmbH Germany 2017

Abstract A three-dimensional groundwater model was used to improve water resource management for a study area in north-west Switzerland, where drinking-water production is close to former landfills and industrial areas. To avoid drinking-water contamination, artificial groundwater recharge with surface water is used to create a hydraulic barrier between the contaminated sites and drinking-water extraction wells. The model was used for simulating existing and proposed water management strategies as a tool to ensure the utmost security for drinking water. A systematic evaluation of the flow direction between existing observation points using a developed three-point estimation method for a large number of scenarios was carried out. It is demonstrated that systematically applying the developed methodology helps to identify vulnerable locations which are sensitive to changing boundary conditions such as those arising from changes to artificial groundwater recharge rates. At these locations, additional investigations and protection are required. The presented integrated approach, using the groundwater flow direction between observation points, can be easily transferred to a variety of hydrological settings to systematically evaluate groundwater modelling scenarios.

Keywords Numerical modelling · Urban groundwater · Groundwater management · Artificial recharge · Switzerland

Electronic supplementary material The online version of this article (doi:10.1007/s10040-017-1640-y) contains supplementary material, which is available to authorized users.

✉ Christian Moeck
Christian.moeck@eawag.ch

[1] Eawag, Swiss Federal Institute of Aquatic Science and Technology, Dübendorf, Switzerland

[2] Department of Environmental Sciences, Applied and Environmental Geology, University of Basel, Basel, Switzerland

[3] Office of Environmental Protection and Energy, Canton Basel-Country, Switzerland

[4] Centre of Hydrogeology and Geothermics (CHYN), University of Neuchâtel, Neuchâtel, Switzerland

Introduction

Proper allocation and management of groundwater is an important and critical challenge under rising water demands of various environmental sectors. Good groundwater quality is however limited because of urbanization and contamination of aquifers in many regions (Singh 2014; Strauch et al. 2008; Tariq et al. 2008). Drinking-water production close to different potential input pathways of contaminants is a common concern for water resource management (Baillieux et al. 2015; Schirmer et al. 2013). It is therefore important to understand the transport and persistence of pollutants in the subsurface to develop adequate groundwater management and protection plans (Levison et al. 2012). Knowledge about flow and transport processes in the subsurface is thus the very basis to develop effective and sustainable water management strategies to protect drinking-water production sites (Doherty and Simmons 2013; Moeck et al. 2016). Typically, groundwater models are used to provide insights about flow and transport processes (Keating et al. 2010). The results of simulation of existing and proposed water management strategies form the basis for the identification of appropriate water management plans for current and future conditions (Singh 2013). Given the predictive capability of groundwater models, they are often the only viable means of providing input to water management decisions, as they can predict the impacts of a specific water management scheme (Gorelick and Zheng 2015).

However, studying and modelling transport processes can be difficult due to the typically unclear distribution and origin of contaminants (Michalak and Kitanidis 2004). Understanding the distribution of contaminants is critical for effective water management, and tracking sources and distribution patterns of contaminants is a challenging task (Hunkeler et al. 2012; Nijenhuis et al. 2013) due to uncertain flow and transport path ways (Srivastava and Singh 2015). The source and distribution pattern can be inversely estimated but is computationally intensive, and obtained results are typically susceptible to errors in the measured data (Milnes and Perrochet 2007; Zhang et al. 2015). Moreover, the monitoring locations can strongly affect the characterization of the unknown contaminant sources and distribution patterns (Jha and Datta 2013). As a result, water-resource-management tasks are based on uncertain assumptions about contaminant distribution patterns and this uncertainty is typically not incorporated into the assessment of risks associated with different proposed management scenarios (Freeze et al. 1990). Here, risk is defined as the probability of unwanted events or system behaviour. Adopted management strategies should be based therefore on a decision-making process that enables a choice to be made between the proposed management strategies while acknowledging the uncertainties of unknown distribution and origin of contaminants.

The objective of this study was to develop a sustainable water-resource-management strategy for a study area in Switzerland, where drinking-water production is close to several former landfills and industrial areas. The study site is characterized by a highly complex geological setting with a partly connected gravel and karst aquifer. To avoid drinking-water contamination, artificial groundwater recharge with surface water into the gravel aquifer is used to create a hydraulic barrier between the contaminated sites and the drinking-water extraction wells. The study seeks to identify the optimum pumping rates at the pumping well gallery as well as infiltration rates and distribution for the artificial groundwater recharge system of channels and ponds. The objective is to ensure that only artificially infiltrated surface water is extracted at the drinking-water pumping-well gallery, to ensure the utmost security for drinking-water production. Regional groundwater from outside of the study area which is potentially contaminated should not be transported towards the pumping well gallery. More specifically, the following research questions and tasks are addressed:

1. Which pumping and infiltration rates lead to a flow direction towards the pumping well gallery?
2. Where are vulnerable locations which are sensitive to changing boundary conditions?
3. Where are locations where additional protection strategies are required apart from adjusting infiltration and pumping rates at the well gallery?
4. What is the most efficient spatial distribution of artificial groundwater recharge within the infiltration system to ensure the utmost security for drinking-water production?
5. For how long is the elevated local groundwater mound present (preventing groundwater flow and transport towards the pumping well gallery) after an infiltration phase has been stopped?

In order to evaluate the large number of modelling scenarios with unknown distribution of contaminants, an automated program code was developed using a three-point estimation method to calculate flow and transport direction within the resulting triangles between the observation points.

Study area

The studied area is located southeast of Basel, Switzerland, and comprises an area of approximately 10 km^2, including urban and industrial zones. Two main aquifers exist, namely the Quaternary sand-gravel and a lower karstified limestone aquifer. The Quaternary sand-gravel aquifer is primarily used for drinking-water production combined with an artificial groundwater recharge system. The infiltration system was designed in order to maintain a hydraulic gradient towards the industrial areas of potential risk and towards the River Rhine (Fig. 1).

Increasing water demand and quality issues led to the installation of the artificial groundwater recharge system. Here, Rhine river water is pumped to an excavated system of channels and seven infiltration ponds to recharge the aquifer (infiltration average is 95,000 m^3/d). Due to the immediate proximity of former landfills and industrial sites, this artificial recharge scheme is used to minimize the risk of drinking-water contamination, which is accomplished by recharging twice as much water as abstracted. This approach of artificial infiltration leads to an elevated local groundwater mound, which serves as a barrier preventing natural inflow of potentially contaminated water coming from adjacent areas (Auckenthaler et al. 2010). To provide further water for industrial use, a pumping well south of the Hardwald area (beneath a landfill site), which has been operated since 1957, is in use. To a great extent, this industrial water use avoids the spreading of contaminated water from the landfill nearby. In addition, large quantities of groundwater are abstracted for industrial purposes east of the study site.

Geological setting of the study area

A large part of the study area is located in the Tabular Jura on the south-eastern shoulder of the Upper Rhine Graben, while the westernmost part of the model area is situated within the Upper Rhine Graben and on the transition zone (“flexure

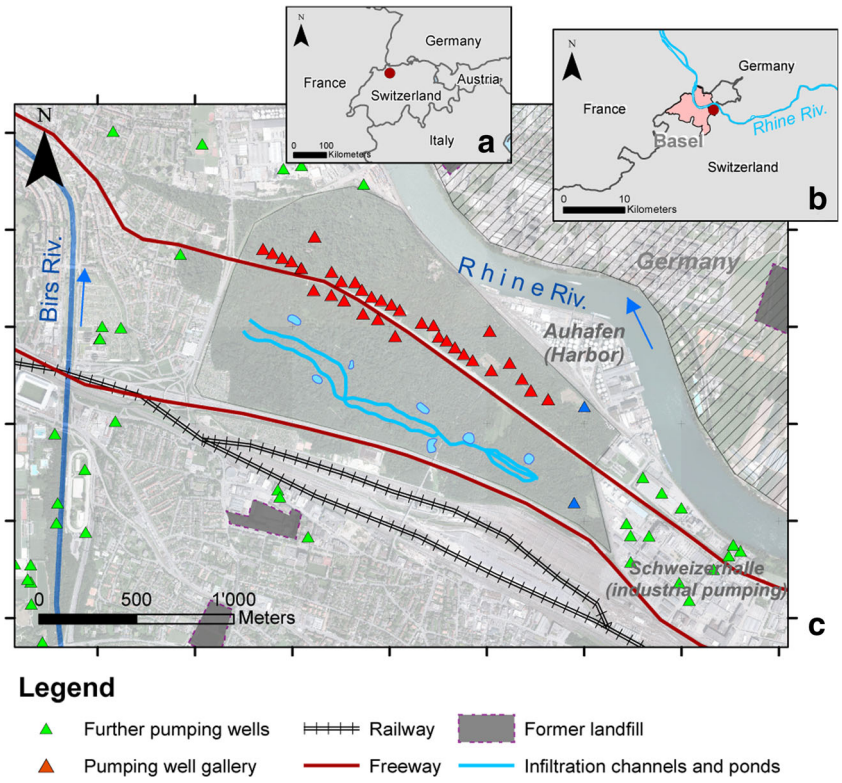

Fig. 1 Study area Hardwald in north-west Switzerland. Elevations range (from south to north) from around 290 m above sea level (masl) to 250 masl in the vicinity of the Rhine River. The northern boundary of the Hardwald area is the *River Rhine*; urban areas and *River Birs* are the boundaries in the west; railways (*tracks*) and *industrial* areas are the boundaries in the south; and industrial areas constitute the boundary in the east. Urban settlements surrounding the study site in the west and the south are illustrated as *grey shaded* areas

zone") to the Tabular Jura (Fig. 2). The most striking tectonic feature of the region is the presence of the main border fault, represented by the flexure zone and a large number of normal faults, mainly orientated in the NNE–SSW direction as well as in the WNW–ESE direction, resulting in faulted blocks, horsts and grabens (Fig. 2).

The hydrogeological sequence relevant to the modelling extends from the Quaternary to the Lower Muschelkalk. The top of the marly Lower Muschelkalk acts as the lower border of the hydrogeological model. It is overlain by the Middle Muschelkalk comprising about 30–130 m of dolomites, marls, clays and evaporates. The Upper Muschelkalk consists mainly of limestone with a thickness of 70–80 m. Together with the ~10-m thick dolomite zone of the Middle Muschelkalk, the limestone of the Upper Muschelkalk represents an important highly fractured and karstified sequence. The following Keuper unit has a thickness of 130–170 m and comprises a series of marls and shales with gypsum and anhydrite lenses and partly dolomites and sandstones. The overlying Jurassic strata are made of 30-m-thick partly porous limestone (Lias) and of an 80–100-m-thick clay layer (Opalinuston). In the study area, the Jurassic strata is present only in the Hardgraben, whilst eroded in the surrounding study area (Bitterli-Brunner and Fischer 1988; Spottke et al. 2005). An unconformity, the bedrock surface, separates the Triassic, Jurassic and Tertiary strata from the unconsolidated Quaternary cover. This cover consists of fluvio-glacial gravel of up to 50-m thickness. The thickness close to the main drinking-water extraction wells (i.e. the pumping well gallery) is around 20–40 m.

Hydrogeology

The groundwater flow in the study area is strongly influenced by the geometry and thickness of the Quaternary alluvial deposits, by the geological structure of the NNE–SSW-trending blocks, horsts and grabens, by the hydraulic boundary conditions, such as the Rhine River level, and by groundwater pumping rates and artificial recharge (Spottke et al. 2005). At Schweizerhalle, an industrial zone in the east (Fig. 1), the Quaternary aquifer and Upper Muschelkalk aquifer are exploited for large-scale industrial water supply. Groundwater modelling reveals that pumping affects the groundwater flow field in the Upper Muschelkalk aquifer at distances of up to 2 km to the south (Spottke et al. 2005). The Quaternary contains unconfined groundwater. The average hydraulic conductivity is in the order of 3.1×10^{-3} m/s (Spottke et al. 2005). The underlying carbonate rocks (limestone, dolomite) and evaporites (gypsum, anhydrite, rock salt) are karstified. This results in the occurrence of different types

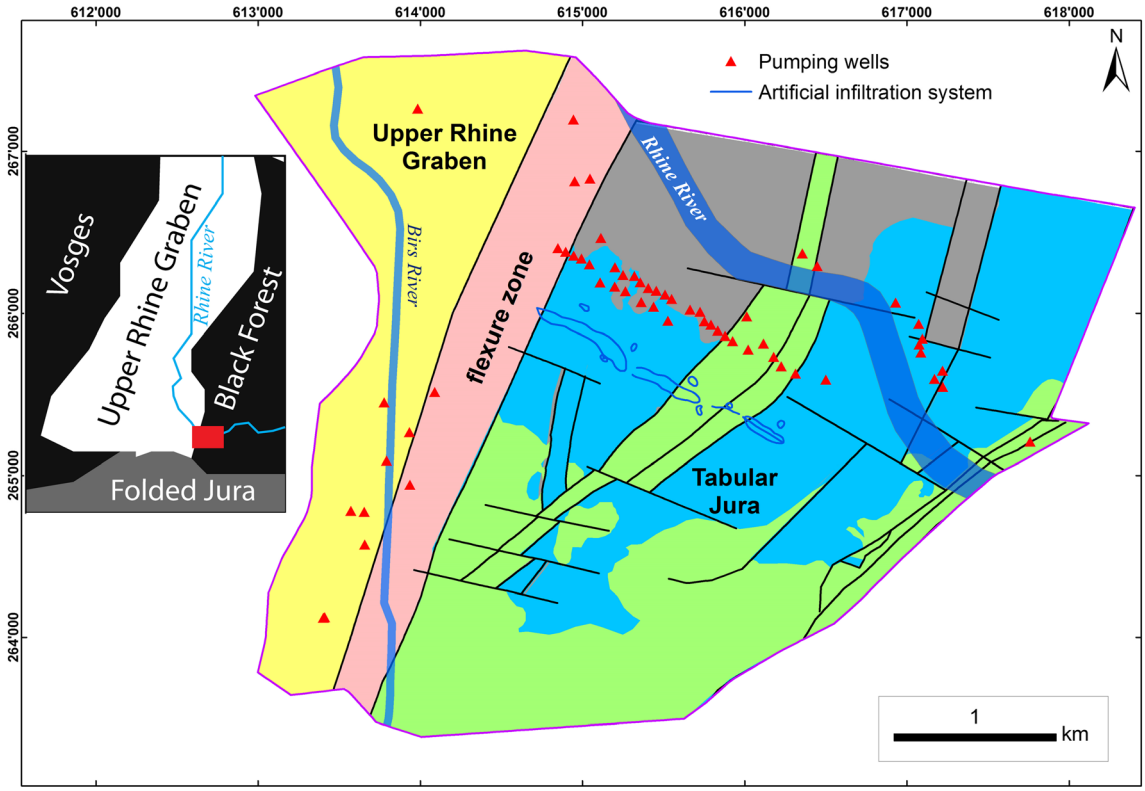

Fig. 2 Bedrock geology, including main faults (*black lines*) of the study area. The bedrock of the Upper Rhine Graben is represented by Tertiary sediments (*yellow*). The composition of the flexure zone is mainly unknown and was not modelled in detail. The bedrock consists of Tertiary and Mesozoic strata (*pink*). The bedrock of the Tabular Jura is made of Triassic to Jurassic sequences: Middle Muschelkalk (*grey*), Upper Muschelkalk (*blue*) and Keuper to Jurassic (*green*)

of aquifer, situated one above the other. The dolomite zone and the limestone of the Upper Muschelkalk represent an important highly fractured and karstified aquifer with a mean hydraulic conductivity of 1.3×10^{-4} m/s (Gürler et al. 1987; Spottke et al. 2005) but within a range between 1×10^{-3} and 2×10^{-6} m/s (Affolter et al. 2010) depending on the location. Due to the dip of the Mesozoic strata, the overlying porous aquifer of the Quaternary and the underlying Triassic karstified Upper Muschelkalk aquifer represent in some places a continuous aquifer in the vertical direction.

The Keuper and Jurassic strata represent aquitards due to their low hydraulic conductivity, between 1.3×10^{-14} and 1.3×10^{-7} m/s. The continuity of the bedrock aquifers is affected by faulting, and these faults may possibly favour the vertical exchange of groundwater across the aquitards (Gürler et al. 1987; Pearson et al. 1991). The hydraulic conductivities of the aforementioned fault zone is unknown and might be variable spatially. The fault zone may present additional flow paths due to increased permeability and therefore may support vertical exchange of groundwater although an aquitard exists (Gürler et al. 1987) or this zone may be filled with fine material and form a hydraulic barrier. The Tertiary sediments which constitute the bedrock of the Upper Rhine Graben represent an aquitard. The composition and also the hydraulic conductivity of the flexure zone is mainly unknown. The intensely structurally deformed zone allows an exchange of groundwater between the bedrock aquifer and the Quaternary sand-gravel aquifer in the western part of the study area.

Methodology

Groundwater model

Previous information from geological (Spottke et al. 2005) and hydrogeological (Butscher and Huggenberger 2007) studies were used to build a three-dimensional (3D) groundwater model for the study area. More than 1,200 drill logs were used to construct the geological model in the software GOCAD (Geological Objects Computer Aided Design), acting as the framework for the groundwater modelling exercise. Six layers with 741,948 nodes and 123,658 elements were incorporated

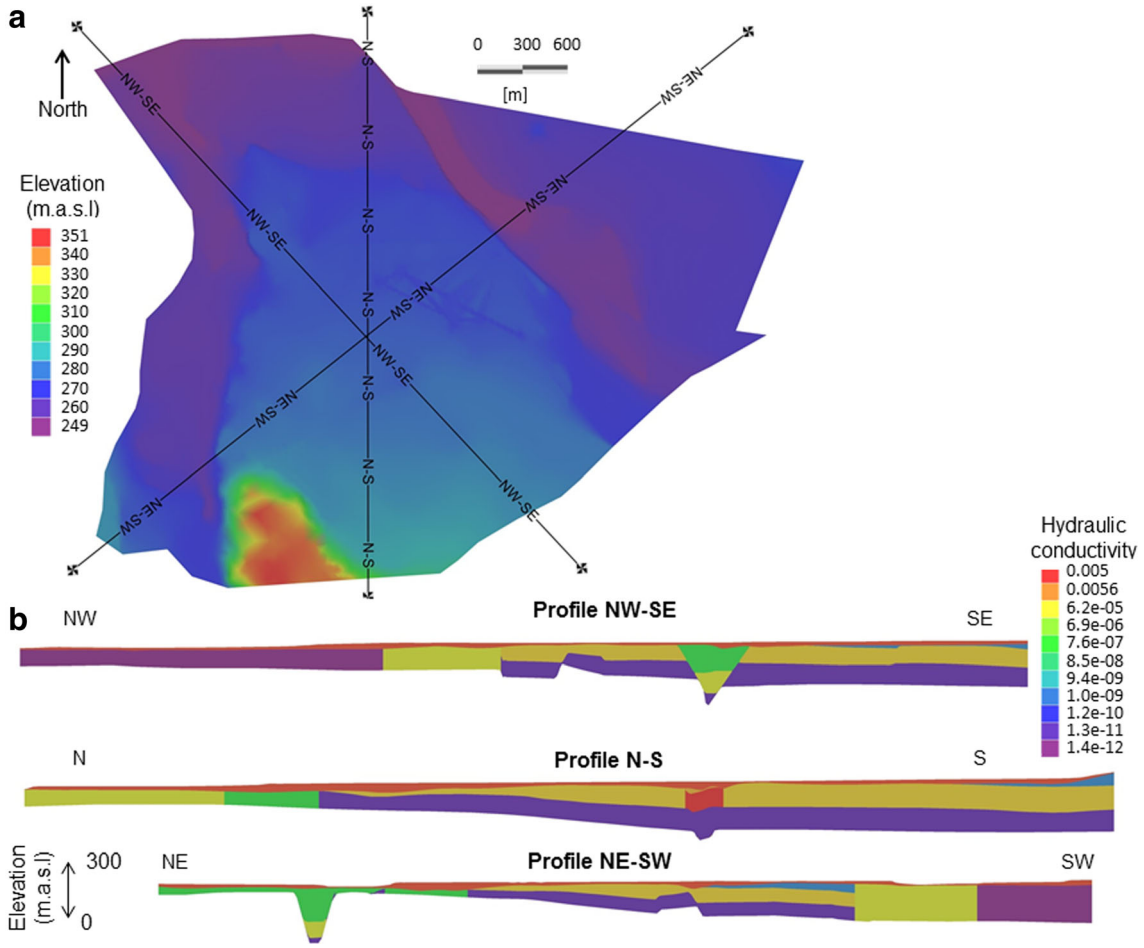

Fig. 3 **a** Plan view of the model area with topographic elevation and three cross-section lines, **b** cross-sections with hydraulic conductivity values [m s^{-1}] representing the different geological units

into the groundwater model (software code FEFLOW, DHI-WASY GmbH) representing the different geological units and tectonic structures (Fig. 3).

Due to the geological and industrial complexity in terms of water extraction in the study area, several different boundary conditions were required (Fig. 4). At the southern border, a constant head (Dirichlet boundary condition) was set between two piezometers. Based on previous investigations (AUG 2009, 2010) model borders in the sand-gravel aquifer in the east and west were described as flux boundaries (Neumann boundary condition) as well as in the bedrock in the south and east. The rivers Rhine and Birs in the north and west, respectively, were implemented as Cauchy boundary condition. An in- and exfiltration rate of 10 d^{-1} was assumed for the River Rhine (AUG 2009, 2010), whereas 35 d^{-1} was set for the River Birs (AUG 2009, 2010). The river stages for the Birs and Rhine were linearly interpolated between four measurement points at different locations for each river. Measurement points were selected based on existing federal measurement stations and before and after artificial barrages along the rivers. All remaining borders were no-flow boundaries. In total 76 pumping wells were included in the numerical model. The 33 Hardwald drinking-water wells (referred to as the 'pumping well gallery') were incorporated into the sand-gravel aquifer in the model. Other wells in the sand-gravel aquifer and bedrock were incorporated into the model too, some of them as multi-level wells, if required. The artificial groundwater recharge rates strongly control the water budget in the study area (Moeck et al. 2017a). Therefore, an inflow on top of the model domain was set as a boundary condition, which represents the infiltration from the artificial groundwater recharge channels and ponds. The average spatial infiltration pattern based on the work of Moeck et al. (2017a) was used. The natural direct groundwater recharge rate was set to 423 mm/year, which is the long-term average for the region (AUG 2010). For sealed areas (impermeable roads, buildings, etc.), a reduced groundwater recharge rate of 171 mm/year was used based on previous work (AUG 2009, 2010). Due to the large amount of artificial groundwater recharge, errors in the provided values of natural groundwater recharge rate had just a minor effect.

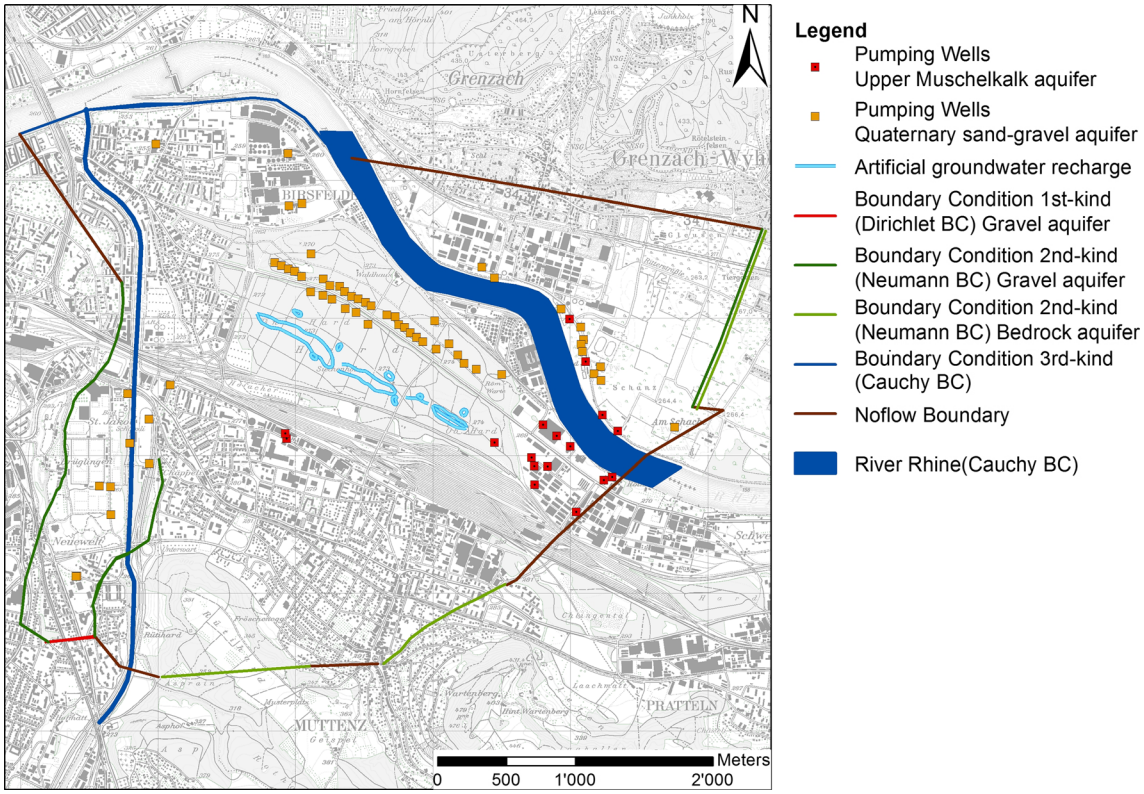

Fig. 4 Model boundary conditions for the study area

A total of 116 piezometers were used for the groundwater model, where 82 piezometers are distributed in the sand-gravel aquifer and 34 in the bedrock. All piezometers were further used for the model calibration discussed in the following section.

Model calibration

The hydraulic conductivity values for the different zones representing the geological units were calibrated with the inverse parameter estimation code PEST (Doherty 2011) on daily piezometer values and under long-term average hydrogeological conditions. For the steady-state calibration, the 116 piezometers were used to minimize the objective target function (∅):

$$\varnothing = \min\left[\sum_{i=1}^{116} w_i\left(h_{\mathrm{obs},i} - h_{\mathrm{sim},i}\right)^2\right] \quad (1)$$

where w is the weight assigned to the piezometric head and the indices obs and sim represent observed and simulated values for the 116 piezometers, respectively. In this study, equal weights were used for all observations. It was assumed that the measurement errors are equal among the different observations and therefore all observation has the same contribution in the objective target function. This weighting strategy is commonly applied in modelling exercises (Foglia et al. 2009; Moeck et al. 2015). Note that the estimated hydraulic conductivity for each geological unit was equal for each model layer.

Model scenarios

The objective of the scenario modelling was to identify boundary conditions that are appropriate for improved water-resource-management strategies. This means that the pumping rates at the pumping well gallery, as well as infiltration rates for the artificial groundwater recharge system of channels and ponds, had to be adjusted with the goal that only artificially infiltrated Rhine river water should be extracted at the well gallery. Regional groundwater flow outside of the Hardwald area, which is potentially contaminated, should not be transported towards the well gallery. Therefore, 476 scenarios with variable pumping and infiltration rates were simulated with the calibrated groundwater model. Pumping and infiltration rates were variable between 0 and 85,000 m^3/d and 0 and 140,000 m^3/d, respectively, in 5,000 m^3/d steps, representing current conditions. The remaining boundary conditions such as industrial pumping were held constant. Furthermore, 100 scenarios were simulated for a redistribution of the artificial infiltration rates. Approximately 75% of

the water currently infiltrates in the eastern part of the infiltration system, whereas only 25% infiltrates in the western part (Moeck et al. 2017a); therefore, in the western part, where the infiltration rates are low, the regional groundwater component is present and drinking-water wells do not only extract artificially infiltrated water (Moeck et al. 2016). Here, the objective was to minimize the influence of the regional groundwater flow by redistributing the artificial infiltration rates which affect the elevated local groundwater mound. The artificial groundwater recharge was variably distributed from east to west under long-term average rates for artificial infiltration and extraction rates at the well gallery. Moreover, an infiltration stop between 1 and 10 days was further simulated to estimate how long the elevated local groundwater mound persists, as well as to estimate the time for recovery. An infiltration stop might be imposed in response to accidental spillage of contaminants upstream in the River Rhine.

Three-point estimation method for risk evaluation

In order to effectively evaluate the risk potential for the study area for the large number of scenarios, an automated code was developed in the open source software 'R' (R Development Core Team 2008), which estimates the horizontal flow direction and magnitude between three observation points. In the work of Pinder et al. (1981) and Devlin and McElwee (2007), it was proposed that the flow direction can be estimated within triangular elements. Devlin (2003) and Devlin and Schillig (2017) presented spreadsheet methods for calculating the hydraulic gradient. This study adapted and further developed that work and coupled it with the numerical model FEFLOW to evaluate the risk potential for the study site. The implementation can be used for other numerical model approaches and can be easily transferred to a variety of hydrological settings.

Under the assumption of a homogenous parameter distribution within the resulting triangle, the flow direction can be expressed as an angle from 0 to 360°, where 90° shows a flow direction to the east and 270 to the west. An angel of 0/360° shows a flow direction towards the north and 180° to the south. The method is graphically illustrated in Fig. 5.

Because the location of each observation point, expressed as the x and y coordinates, as well as the piezometric head (h) is known, a two-dimensional plane based on three observation points can be calculated.

$$h_i(x,y) = a + bx_i + cy_i \tag{2}$$

The resulting linear equations can be solved inversely for factors a, b and c for the x and y coordinates of the observation point i = 1, 2 and 3

$$\begin{aligned} h_1 &= a + bx_1 + cy_1 \\ h_2 &= a + bx_2 + cy_2 \\ h_3 &= a + bx_3 + cy_3 \end{aligned} \tag{3}$$

The head gradient in x (J_x) and y (J_y) coordinate can be expressed as:

$$J_x = -\frac{\partial h}{\partial x} = -b \tag{4}$$

$$J_y = -\frac{\partial h}{\partial y} = -c \tag{5}$$

Subsequently the angle of the head gradient can be calculated with an arc tangent function:

$$\theta = \tan^{-1}\left(\frac{c}{b}\right) = \tan^{-1}\left(\frac{J_y}{J_x}\right) = \tan^{-1}\left(\frac{\partial h/\partial y}{\partial h/\partial x}\right) \tag{6}$$

Whereas the magnitude of the head gradient can be calculated with the following equation:

$$|J| = \sqrt{b^2 + c^2} \tag{7}$$

The method was applied in the Hardwald study area by using the large number of existing piezometers. Due to the calculation of the flow direction within the three-point estimation method (creating triangles) for the aforementioned different scenarios, it was possible to carry out a systematic evaluation. Overall, 32 triangles were created covering the entire area around Hardwald (Fig. 6). For each triangle, two subgroups of flow direction were applied to evaluate the risk potential under different scenarios. A groundwater flow direction towards the pumping well gallery in the Hardwald area indicates a potential risk (red area of the circle), whereas for the reverse flow direction, a risk is unlikely (green area of the circle). Note that the method does not take dispersion and vertical transport into account. These limitations have to be considered if the method is applied at other study areas where advective transport is not the only controlling process for pollution migration. Furthermore, results can be influenced by poor hydraulic connection of the observation well, leading to biased water-table heads; moreover, measurement errors can lead to misleading gradient calculations when water level differences between the wells are too small (Devlin and Schillig 2017).

Results

Calibration

Figure 7 shows the scatter plot between observed (x-axis) and simulated (y-axis) groundwater heads for the 116 piezometers. The piezometers in the top sand-gravel aquifer are shown as triangles, whereas the piezometers in the bedrock are displayed as rectangles. Generally, a good fit was achieved and no systematic over or under estimation occurred. The percentage of bias (PBIAS) is only 0.1% and a correlation of

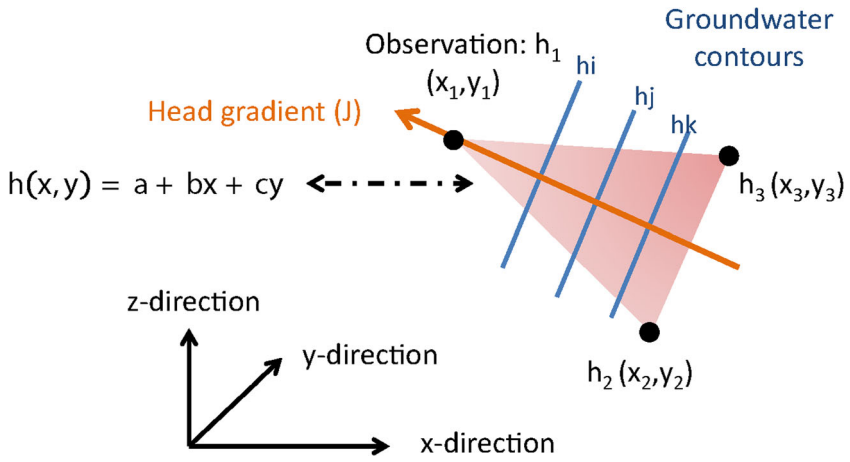

Fig. 5 Graphical illustration of the three-point method that builds the basis for the developed R-code to estimate horizontal flow direction and magnitude between three observation points

0.95 was obtained during the calibration. The residuals (small grey panel in Fig. 6) show errors between 0 and ±0.5 m. The spatial distribution of the residuals shows a small overestimation of the piezometric head south of the pumping well gallery. A small underestimation occurred in the eastern part of the study area. The assumption of zones of piecewise constancy of the hydraulic conductivity can lead to local mismatches between observed and simulated groundwater heads due to simplification of subsurface heterogeneity (Moeck et al. 2015; Moore and Doherty 2006). However, taking into account the different water uses and particularly the huge amounts of extraction and infiltration in the study area, these

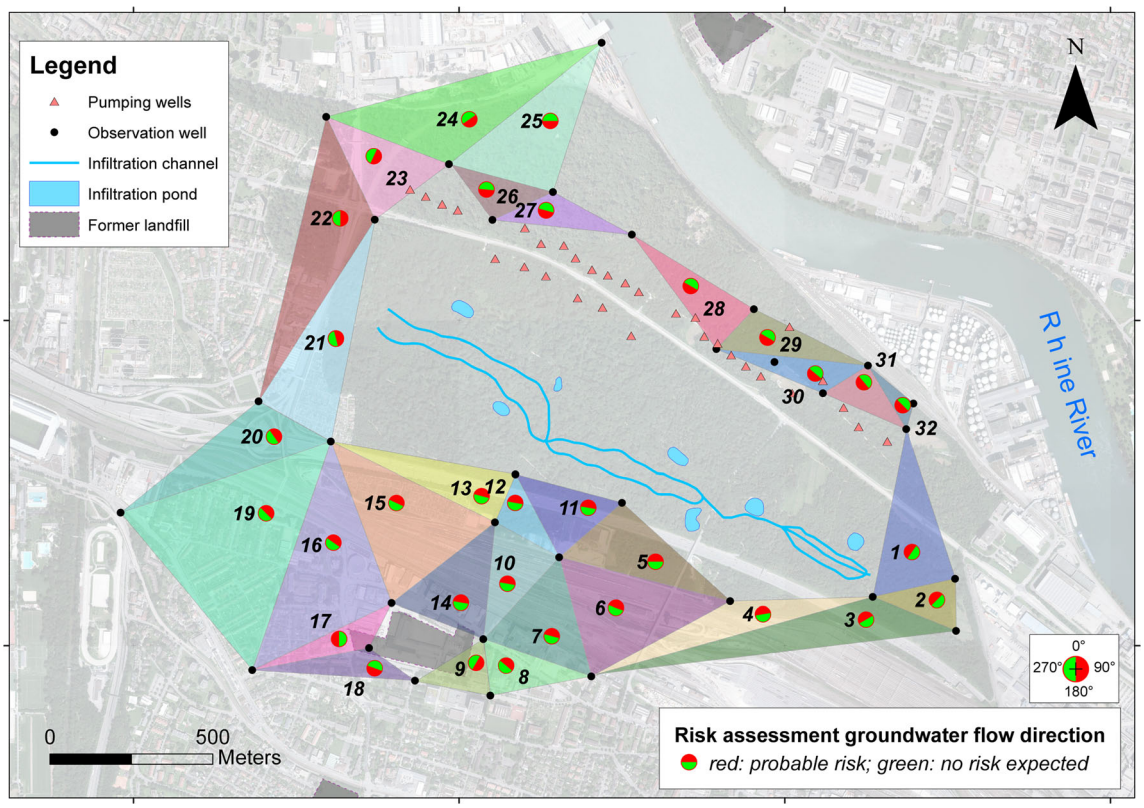

Fig. 6 Generated triangles between piezometers in which the flow direction is calculated. A groundwater flow direction towards the pumping well gallery in the Hardwald area indicates a potential risk (*red area of the circle*), whereas for the reverse flow direction a risk is unlikely (*green area of the circle*)

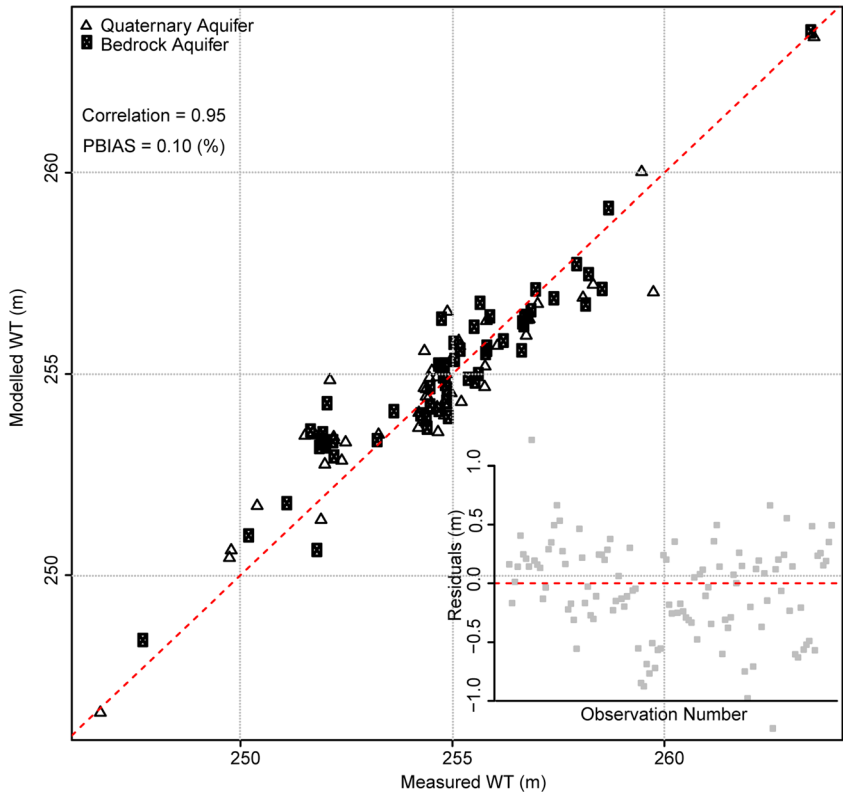

Fig. 7 Measured water table (*WT*) versus modelled water table (WT) elevation for the Quaternary aquifer (*triangles*) and bedrock aquifer (*rectangles*). The residuals are shown in the *small panel* where observed minus simulated heads are displayed

errors seem to be acceptable—see Fig. S1 of the electronic supplementary material (ESM). The resulting hydraulic conductivities for each zone from the calibration exercise are displayed in the supporting information (Figs. S2–S6 of the ESM).

Variable pumping and infiltration rates

The results for three different triangles are shown in the following as an example (Fig. 8). These triangles represent the system behaviour for different spatial locations. The remaining results for the other triangles are provided in the supporting information (Figs. S8–S23 of the ESM). The differences relative to the optimum flow angle for the triangles 4 (south-east), 17 (south-west) and 28 (north) are displayed in Fig. 8. In case of an angle of 0°, the optimum is reached (green colour), meaning that there is a reverse groundwater flow direction relative to the flow direction towards the pumping well gallery. Differences larger than 90° indicate a groundwater flow direction from outside of the Hardwald area towards the pumping well gallery. Here, a potential risk originating from contaminated areas is possible (yellow to red colour). The blue points show the daily infiltration and pumping rates during the time period 2008–2014.

For triangle 4, only when the pumping rate is high and infiltration is low, a flow direction towards the pumping well gallery occurred (Fig. 8). For most scenarios, the reverse flow direction relative to the pumping well gallery is the objective flow direction. The flow direction in the south-eastern area is most likely also controlled by industrial pumping in the east, where high amounts of up to 42,000 m^3/d of groundwater is extracted. Therefore, variable pumping or infiltration in the Hardwald area has just a minor influence on the flow direction. For triangle 17, the optimum flow direction is towards the former landfill in the east. At the landfill, groundwater is additionally extracted to avoid a down-gradient flow from the landfill to the western border of the study area which might influence water quality at the pumping wells located at the western edge of the pumping well gallery. However, for average conditions of infiltration and pumping this is not observed. A high infiltration leads to an elevated local groundwater mound, which leads to down-gradient flow to the western direction. Higher pumping rates and lower infiltration would lead to the desired flow direction towards the east. Previous investigations came to a similar result (AUG 2010). They showed that the flow direction is towards the landfill when no infiltration occurred and when pumping at the landfill is active. Reducing the infiltration rate would help to maintain a flow direction towards the landfill locally. For the bulk of triangles, this leads, however, to a flow in the direction of the pumping well gallery. Here, industrial pumping at the landfill must be increased to avoid down-

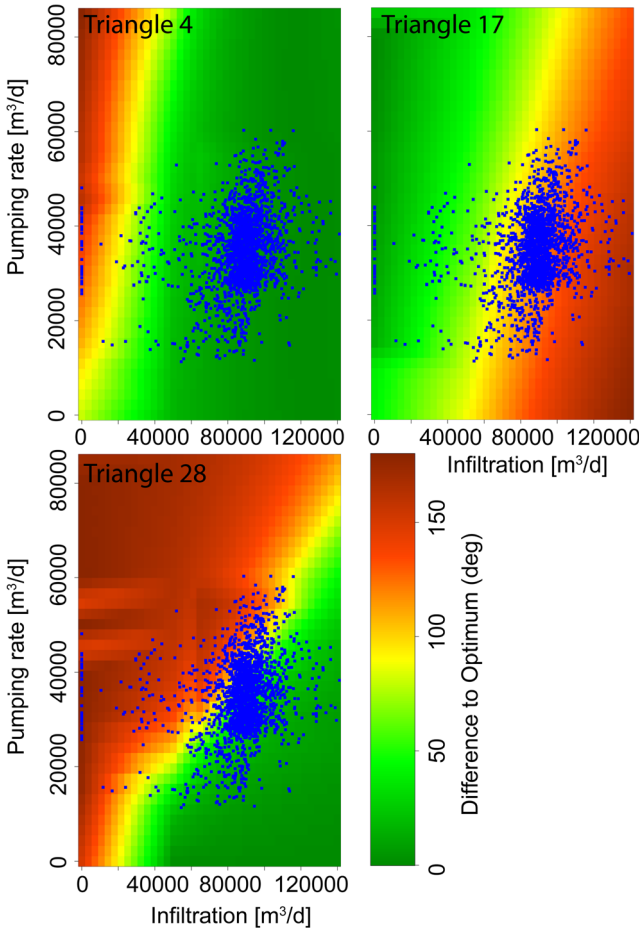

Fig. 8 Interpolated differences relative to the optimum flow angle for triangle 4 (south-east), 17 (south-west) and 28 (north). The *x-axis* shows the infiltration rate (m^3/d), whereas on the *y-axis* the pumping rates (m^3/d) for the well gallery are displayed. In the case of an angle of 0°, the optimum is reached (*green colour*), meaning that the groundwater flow direction is the reverse of the direction to the pumping well gallery. Difference > 90° indicates a groundwater flow direction from outside of the Hardwald area towards the pumping well gallery. A potential risk originating from contaminated areas is possible (*yellow to red colour*). The *blue points* show the daily infiltration and pumping rates during the time period 2008–2014

gradient flow. For triangle 28, a strong dependence of the flow direction on the pumping and infiltration rates can be observed. The combination of infiltration and pumping rates which leads to a flow direction towards the pumping well gallery are larger compared to the other two triangle examples. Higher pumping rates with low or average infiltration rates leads to flow towards the pumping well gallery. Certainly, the location of the triangle in the close vicinity of the pumping wells induces a stronger dependency of changing boundary conditions. Only with higher infiltration rates is a reverse flow direction to the well gallery obtained.

Overall, under average pumping and infiltration rates (infiltration of 95,000 m^3/d and pumping rate of 45,000 m^3/d), the flow direction is reverse relative to the flow direction towards the drinking-water pumping well gallery. The risk for an intake of regional contaminated groundwater into the drinking-water wells is relatively low. Apart from that, the method helps to identify vulnerable locations which are sensitive to changing boundary conditions and where additional protection is required such as higher industrial pumping rates in the vicinity of triangle 17.

Distribution of infiltration rates

Due to the unequal infiltration distribution (75% in the east and 25% in the west of the infiltration system (Moeck et al. 2017a), the effect of a redistribution of the infiltration was simulated. The total infiltration was 95,000 m^3/d and the abstraction at the pumping well gallery was 45,000 m^3/d, which is the long-term average condition. All triangles were considered, to identify the optimum infiltration distribution. The sum of the differences relative to the optimum flow angle for each triangle was calculated with the following equation.

$$\varnothing = \min\left[\sum_{i=1}^{n} w_i \left(D_{\mathrm{opt}_i} - D_{\mathrm{s}_i}\right)^2\right] \quad (8)$$

The goal was to find a minimum target function (∅) which shows the best result for all triangles in terms of flow direction. The factor w_i is the weighting for all 32 triangles. An identical weight was chosen for all triangles leading to no preferential spatial optimization. Note that with an adapted weighting strategy, a focus on preferential spatial location can be carried out. The overall objective was that groundwater from outside of the Hardwald area, where the groundwater is potentially contaminated, is not transported towards the pumping well gallery. Therefore, the differences between the optimum angle (D_{opt_i}) and simulated angle (D_{s_i}) were calculated.

Figure 9 shows the results of the simulations where on the x-axis the infiltration rates are presented for the eastern and western part of the infiltration system. The y-axis shows the normalized target function. Every target function was divided by the maximum achieved target function obtained for all simulations. A value of 1, therefore, shows the poorest result, whereas a value smaller than 1 indicates an improvement. It can be seen that infiltration just in the eastern or western part does not lead to the desired flow direction. A more balanced distribution between the eastern and western part of the artificial infiltration system leads to the best result. A value of 42% infiltration in the western part and 58% in the eastern part of the infiltration system leads to the optimal result.

Artificial groundwater recharge interruption

Here scenarios were simulated to estimate systematically the effect of an infiltration stop. An infiltration stop might occur

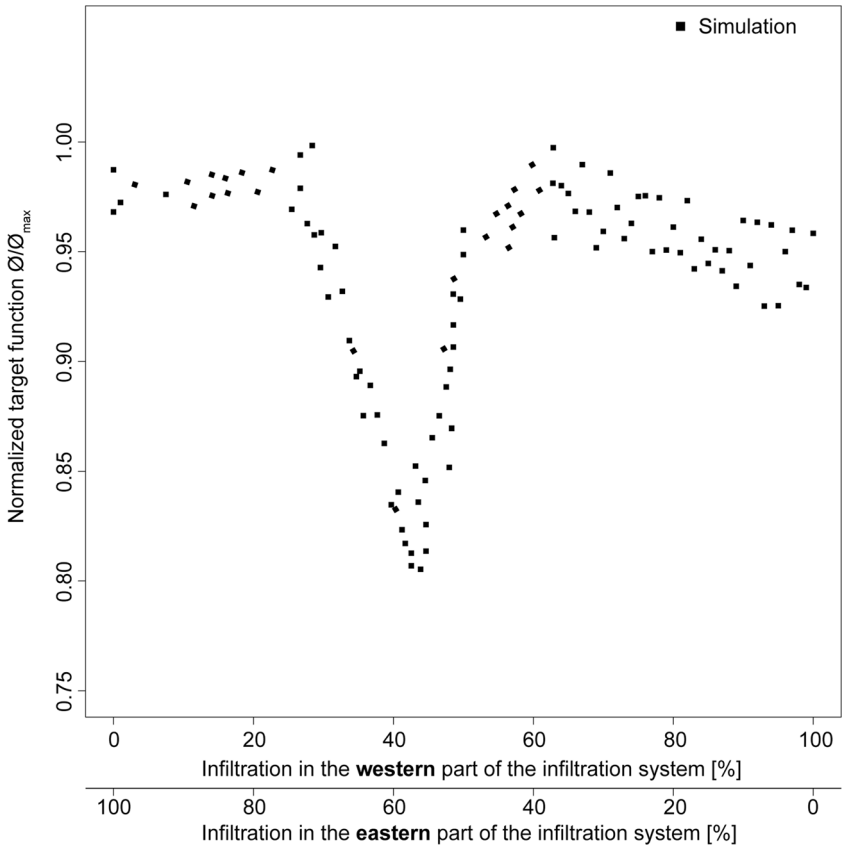

Fig. 9 Infiltration pattern of the artificial groundwater recharge system between western and eastern part. The *y-axis* shows the normalized target function

due to spillage of contaminants upstream in the River Rhine (Moeck et al. 2017a). The distribution of the artificial infiltration represents the current conditions and not the aforementioned redistribution. An important question is the period of time over which the elevated local groundwater mound exists under an infiltration stop, preventing groundwater flow and transport towards the pumping well gallery. Additionally, the speed of return of the water-table height after infiltration resumes is of particular interest for water management in the study area.

In the following, the results for an infiltration of 95,000 m^3/d and a pumping rate of 45,000 m^3/d are described. This scenario represents a realistic, currently used rate. Figure 10a shows the interpolated water table for an infiltration stop of 1 day. Four time steps are presented, where t0 shows the water-table elevation—m above sea level (masl)—before the infiltration stop. Time step t1 represents the period (1 day) during which the infiltration was stopped, and time step t2 displays the water table when the infiltration was again activated. The end of time step t4 represents the water-table behaviour three full days after reactivating the infiltration. Before the infiltration stop (t0) the elevated local groundwater mound is presented where a higher water table occurred in the eastern part of the infiltration system due to the unbalanced infiltration rate. The hydraulic barrier is therefore most efficient in the eastern part. Pumping wells located west within the pumping well gallery have therefore a higher risk potential than wells in the east. This finding is in line with previous work based on field data analysis (Moeck et al. 2016, 2017a). For time step t1, a decrease in the water table can be observed. The water table is however still higher than the surrounding heads. Therefore, the hydraulic barrier is still present. During time step t2, where infiltration has been reactivated, a fast return of the water-table height can be observed until the original conditions are obtained again (t4).

Figure 10b shows the interpolated water table for an infiltration stop of 5 days. The time t0 shows again the water table before the infiltration stop. Time step t1 shows the time period when the infiltration has been stopped, whereas for time step t2, the infiltration is still not active. The time step t4 shows the water-table behaviour 4 days after interruption of the infiltration. Still no infiltration occurred but pumping is continuously active. For t0, the same elevated local groundwater mound can be observed as seen for the previous scenario with an infiltration stop of 1 day. For time step t1, an ongoing decrease in the water table can be observed. During time step t2, where infiltration is still not activated, a continuous decrease of the water table can be observed. The effect of the hydraulic barrier has considerably decreased and flow from the south to the north

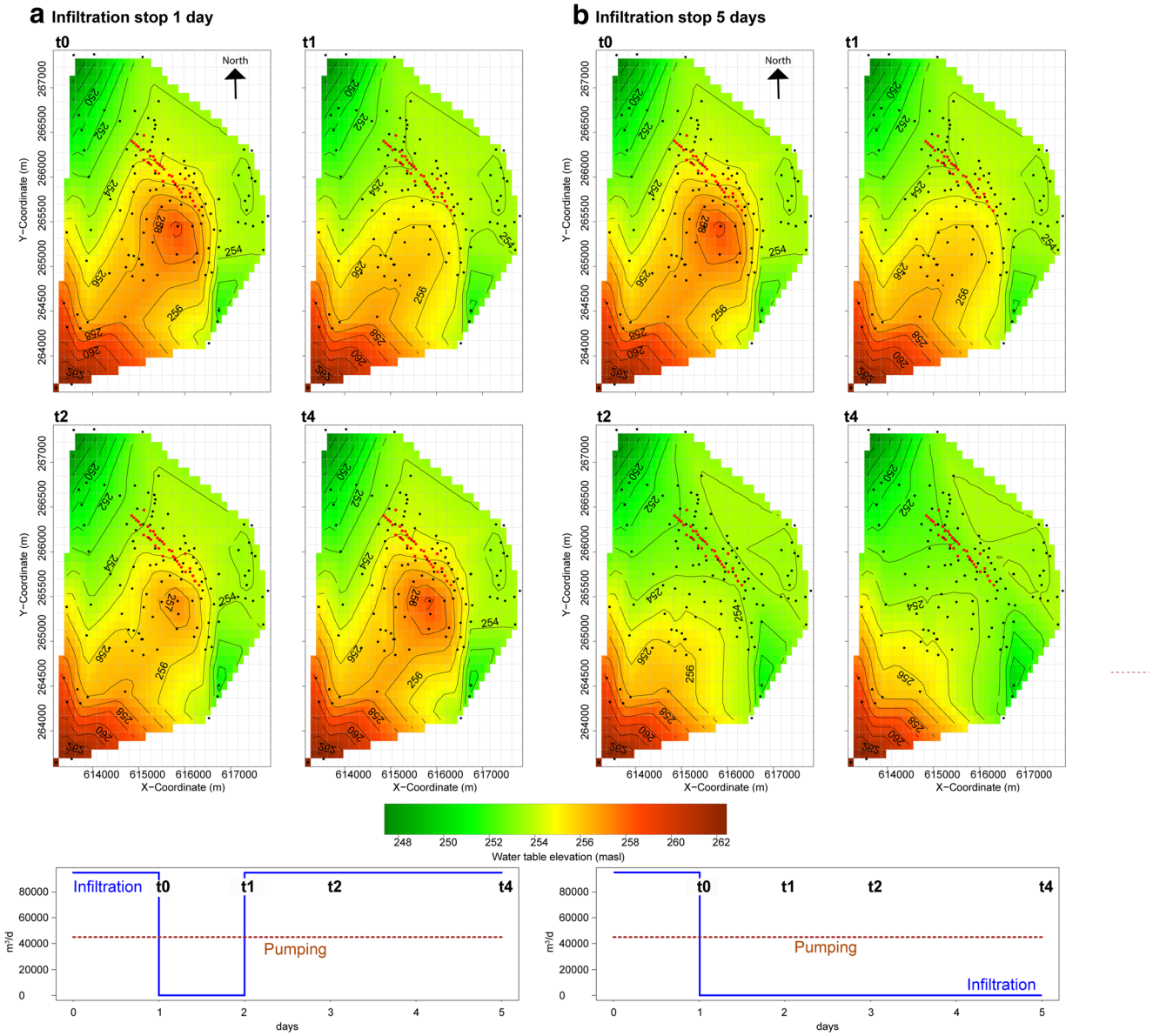

Fig. 10 Water-table elevation for time steps 0–4 for an infiltration stop of **a** 1 day and **b** 5 days. *Green colour* shows lower water-table elevation, whereas *red colour* shows higher water-table elevation

towards the Rhine through the Hardwald area is possible; also, a flow from the north to the pumping well gallery can be observed. During time step t4, the hydraulic barrier completely disappears and a steady-state flow field from south to north arises.

Overall, a stop of the infiltration longer than 4 days should be avoided. A longer interruption, which might be necessary to manage a pollution event in the Rhine river water (thereby avoiding contaminants entering the aquifer), can lead to gradual flow from the south (where contaminated areas exist) towards the north through the Hardwald area. This is in line with field data analysis based on information gained from seven different tracers during a pumping experiment (Moeck et al. 2017a). Longer infiltration stops are not shown because the results and conclusions are the same. An infiltration stop is a critical water resource management option at the study site. However, the return to the necessary water-table height, and therefore the hydraulic barrier, occurred relatively fast, within 1–2 days after the infiltration is reactivated.

Summary and conclusion

tyIn this study, a 3D groundwater model was used to improve water resource management for a study area, where drinking-water production is close to former landfills and industrial areas. To avoid drinking-water

contamination, artificial groundwater recharge with surface water into the gravel aquifer is used to create a hydraulic barrier between contaminated sites and drinking-water extraction wells. The calibrated model was used for simulating existing and proposed water-management strategies as a tool to ensure the utmost security for drinking water. A systematic evaluation of the flow direction between three observation points (creating a triangle) for a large number of scenarios was carried out. Due to the numerous observation points, 32 triangles were created which cover the entire area around the study site. For each triangle, two subgroups of flow direction were applied to evaluate the risk potential under different scenarios. A groundwater flow direction towards the pumping well gallery in the Hardwald area indicates a potential risk, whereas for the reverse flow direction the risk is very low.

For the specific study site the following conclusions can be drawn. Under average pumping and infiltration rates, the flow direction is away (i.e. reverse direction) from the drinking-water pumping well gallery and the elevated local groundwater mound, which serves as a barrier preventing natural inflow of potentially contaminated water coming from adjacent areas. In this case, the risk potential is relatively low for the drinking-water wells. However, increasing pumping rates or decreasing infiltration (alone or in combination) lead to an increasing risk potential. Flow directions within triangles in the eastern part of the study area are not only controlled by changing infiltration and pumping rates of the pumping well gallery; industrial pumping strongly controls the groundwater flow too. Similar results are obtained for the flow directions for triangles in the vicinity of the former landfill in the south. Although a higher sensitivity of the flow direction on changing infiltration and pumping rates of the pumping well gallery can be observed, a down-gradient flow from the landfill towards the western direction of the study area can only be avoided when industrial pumping is increased. In addition, the highest sensitivity with respect to the flow direction, when changing infiltration and pumping rates of the pumping well gallery, is present in the northern part of study area. Furthermore, a balanced infiltration pattern between the eastern and western sections of the infiltration system leads to a more optimum distribution of the elevated local groundwater mound, whereas an infiltration just in the eastern (or western) part does not lead to the desired flow directions. In addition, an infiltration stop of longer than 4 days should be avoided to minimize the risk of flow from south towards the north through the study site. However, the return of the water-table height and therefore the hydraulic barrier occurred relatively fast, within 1–2 days after the infiltration is reactivated.

In this study, it was demonstrated that systematically applying the developed three-point estimation method helps to identify important locations which are sensitive to changing boundary conditions and where additional protection is required. With new sensor techniques that offer remote access, the water supplier can easily install flow sensors in existing piezometers at important locations and can observe directly how the flow angle is changing due to changes in the pumping and/or infiltration rates. The beauty of this approach is the simplicity compared to complex flow and transport modelling which is commonly not possible for water suppliers due to time and manpower restrictions. Furthermore, the presented approach, using the flow direction between three observation points, can be easily transferred to a variety of hydrological settings to evaluate different groundwater modelling scenarios at the same time.

Acknowledgements The authors acknowledge the financial support from the Canton Basel-Landschaft, Switzerland, in the framework of the project "Regionale Wasserversorgung Basel-Landschaft 21" as well as internal Eawag Discretionary Funding. This study was also supported by the Competence Center Environment and Sustainability (CCES) of the ETH domain in the framework of the RECORD Catchment project (coupled ecological, hydrological and social dynamics in restored and channelized corridors of a river at the catchment scale). The AE and two anonymous reviewers are greatly appreciated for their constructive comments.

References

Affolter A, Huggenberger P, Zechner E (2010) Grundwassermodell Unteres Birstal- Rhein - Muttenz: Evaluation der Zustrombereiche der Trinkwasserfassung Muttenz und Hardwasser AG [Groundwater model Unteres Birstal- Rhein - Muttenz: Evaluation of the inflow zone of the drinking water supply system Muttenz and Hardwasser AG]. Report. BL-155, BGA

Auckenthaler A, Baenninger D, Affolter A, Zechner E, Huggenberger P (2010) Drinking water production close to contaminant sites: a case study from the region of Basel, Switzerland. GQ10: groundwater quality management in a rapidly changing world. Proc. 7th International Groundwater Quality Conference held in Zurich, Switzerland, 13-18 June 2010. IAHS Publ. 342 (2011), pp 167-170

AUG (Angewandte und Umweltgeologie der Universität Basel) (2009) Stationär kalibriertes Grundwassermodell Muttenz unteres Birstal: Berechnung geschichtlicher Szenarien zur Abschätzung der Schadstoffverteilung der Deponien in Muttenz [Steady-state calibrated groundwater model for Muttenz unteres Birstal: historical scenarios for the evaluation of contaminant distribution in the landfill in Muttenz]. Report BGA BL-155, AUG, Basel, Switzerland

AUG (Angewandte und Umweltgeologie der Universität Basel) (2010) Grundwassermodell Unteres Birstal - Rhein - Muttenz: Evaluation der Zuströmbereiche der Trinkwasserfassungen Muttenz und Hardwasser AG [Groundwater model for Unteres Birstal - Rhein - Muttenz: evaluation of the inflow areas of drinking water sites Muttenz and Hardwasser AG]. Report BGA BL-155, AUG, Basel, Switzerland

Baillieux A, Moeck C, Perrochet P, Hunkeler D (2015) Assessing groundwater quality trends in pumping wells using spatially varying transfer functions. Hydrogeol J 23:1449–1463

Bitterli-Brunner P, Fischer H (1988) Blatt 1067 Arlesheim: Erläuterungen, Geologischer Atlas der Schweiz 1:25′000 [Sheet 1067, Arlesheim: explanations, geological atlas of Switzerland1:

25,000]. National Hydrological and Geological Survey, Bern, Switzerland

Butscher C, Huggenberger P (2007) Implications for karst hydrology from 3D geological modeling using the aquifer base gradient approach. J Hydrol 342:184–198

Devlin JF (2003) A spreadsheet method of estimating best-fit hydraulic gradients using head data from multiple wells. Ground Water 41(3): 316–320

Devlin JF, McElwee CD (2007) Effects of measurement error on horizontal hydraulic gradient estimates. Ground Water 45(1):62–73

Devlin JF, Schillig PC (2017) HydrogeoEstimatorXL: an Excel-based tool for estimating hydraulic gradient magnitude and direction. Hydrogeol J 25:867. doi:10.1007/s10040-016-1518-4

Doherty JE (2011) PEST: model-independent parameter estimation, user manual. Watermark, Brisbane, Australia. Available at http://www.pesthomepage.org/Downloads.php. Accessed 20 Nov 2016

Doherty J, Simmons CT (2013) Groundwater modelling in decision support: reflections on a unified conceptual framework. Hydrogeol J 21: 1531–1537

Foglia L, Hill MC, Mehl SW, Burlando P (2009) Sensitivity analysis, calibration, and testing of a distributed hydrological model using error-based weighting and one objective function. Water Resour Res 45:627–641

Freeze RA, Massmann J, Smith L, Sperling T, James B (1990) Hydrogeological decision-analysis, 1: a framework. Ground Water 28:738–766

Gorelick SM, Zheng C (2015) Global change and the groundwater management challenge. Water Resour Res 51:3031–3051. doi:10.1002/2014WR016825

Gürler B, Hauber L, Schwander M (1987) Die Geologie der Umgebung von Basel mit Hinweisen über die Nutzungsmöglichkeiten der Erdwärme, Beiträge zur Geologischen Karte der Schweiz [Geology of Basel and surroundings, including remarks on the potential of geothermal energy use: contribution to the geological map of Switzerland]. National Hydrological and Geological Survey Geotechnical Committee, Bern, Switzerland

Hunkeler D, Laier T, Breider F, Jacobsen OS (2012) Demonstrating a natural origin of chloroform in groundwater using stable carbon isotopes. Environ Sci Technol 46:6096–6101

Jha M, Datta B (2013) Three-dimensional groundwater contamination source identification using adaptive simulated annealing. J Hydrol Eng18. doi:10.1061/(ASCE)HE.1943-5584.0000624

Keating EH, Doherty J, Vrugt JA, Kang QJ (2010) Optimization and uncertainty assessment of strongly nonlinear groundwater models with high parameter dimensionality. Water Resour Res 46: W10517. doi:10.1029/2009WR008584

Levison J, Novakowski K, Reiner E, Kolic T (2012) Potential of groundwater contamination by polybrominated diphenyl ethers (PBDEs) in a sensitive bedrock aquifer (Canada). Hydrogeol J 20:401–412. doi: 10.1007/s10040-011-0813-3

Michalak AM, Kitanidis PK (2004) Estimation of historical groundwater contaminant distribution using the adjoint state method applied to geostatistical inverse modeling. Water Resour Res 40:W08302

Milnes E, Perrochet P (2007) Simultaneous identification of a single pollution point-source location and contamination time under known flow field conditions. Adv Water Resour 30:2439–2446

Moeck C, Hunkeler D, Brunner P (2015) Tutorials as a flexible alternative to GUIs: an example for advanced model calibration using pilot points. Environ Model Softw 66:78–86

Moeck C, Radny D, Borer P, Rothardt J, Auckenthaler A, Berg M, Schirmer M (2016) Multicomponent statistical analysis to identify flow and transport processes in a highly complex environment. J Hydrol 542:437–449

Moeck C, Radny D, Auckenthaler A, Berg M, Hollender J, Schirmer M (2017a) Estimating spatial distribution of artificial groundwater recharge using multiple tracers. Isot Environ Health Stud. doi: 10.1080/10256016.2017.1334651

Moeck C, Radny D, Popp A, Brennwald M, Stoll S, Auckenthaler A, Berg M, Schirmer M (2017b) Characterization of a managed aquifer recharge system using multiple tracers. Sci Total Environ. doi:10.1016/j.scitotenv.2017.07.211

Moore C, Doherty J (2006) The cost of uniqueness in groundwater model calibration. Adv Water Resour 29:605–623

Nijenhuis I, Schmidt M, Pellegatti E, Paramatti E, Richnow HH, Gargini A (2013) A stable isotope approach for source apportionment of chlorinated ethene plumes at a complex multi-contamination events urban site. J Contam Hydrol 153:92–105. doi:10.1016/j.jconhyd.2013.06.004

Pearson FJ Jr, Balderer W, Loosli HH, Lehmann BE, Matter A, Peters TJ, Schmassmann H, Gautschi A (eds) (1991) Applied isotope hydrogeology: a case study in northern Switzerland. Studies in Environmental Sciences, vol 43. Elsevier, Amsterdam

Pinder GF, Celia M, Gray WG (1981) Velocity calculation from randomly located hydraulic heads. Ground Water 19(3):262–264

R Development Core Team (2008) R: A language and environment for statistical computing. R Foundation for Statistical Computing, Vienna, Austria. http://www.R-project.org

Schirmer M, Leschik S, Musolff A (2013) Current research in urban hydrogeology: a review. Adv Water Resour 51:280–291

Singh A (2013) Groundwater modelling for the assessment of water management alternatives. J Hydrol 481:220–229. doi:10.1016/j.jhydrol.2012.12.042

Singh A (2014) Simulation–optimization modeling for conjunctive water use management. Agric Water Manage 141:23–29. doi:10.1016/j.agwat.2014.04.003

Spottke I, Zechner E, Huggenberger P (2005) The southeastern border of the upper Rhine Graben: a 3D geological model and its importance for tectonics and groundwater flow. Int J Earth Sci 94:580–593

Srivastava D, Singh RM (2015) Groundwater system modeling for simultaneous identification of pollution sources and parameters with uncertainty characterization. Water Resour Manag 29:4607–4627. doi: 10.1007/s11269-015-1078-8

Strauch G, Möder M, Wennrich R, Osenbrück K, Gläser H-R, Schladitz T, Müller C, Schirmer K, Reinstorf F, Schirmer M (2008) Indicators for assessing anthropogenic impact on urban surface and groundwater. J Soils Sediments 8:23–33

Tariq SR, Shah MH, Shaheen N, Jaffar M, Khalique A (2008) Statistical source identification of metals in groundwater exposed to industrial contamination. Environ Monit Assess 138:159–165

Woodbury AD, Sudicky EA (1991) The geostatistical characteristics of the Borden aquifer. Water Resour Res 27:533–546

Zhang J, Zeng L, Chen C, Chen D, Wu L (2015) Efficient Bayesian experimental design for contaminant source identification. Water Resour Res 51:576–598. doi:10.1002/2014WR015740